Graefe's Archive for Clinical and Experimental Ophthalmology (2018) 256:341–353
https://doi.org/10.1007/s00417-017-3883-7

BASIC SCIENCE

Comparison of the neuroinflammatory responses to selective retina therapy and continuous-wave laser photocoagulation in mouse eyes

Jung Woo Han[1] · Juhye Choi[2] · Young Shin Kim[1] · Jina Kim[1] · Ralf Brinkmann[3] · Jungmook Lyu[2] · Tae Kwann Park[1,4,5]

Received: 1 July 2017 / Revised: 2 November 2017 / Accepted: 20 December 2017 / Published online: 10 January 2018

Abstract

Purpose This study investigated microglia and inflammatory cell responses after selective retina therapy (SRT) with microsecond-pulsed laser in comparison to continuous-wave laser photocoagulation (cwPC).

Methods Healthy C57BL/6 J mice were treated with either a train of short pulses (SRT; 527-nm, Q-switched, 1.7-μs pulse) or a conventional thermal continuous-wave (532-nm, 100-ms pulse duration) laser. The mice were sacrificed and their eyes were enucleated 1, 3, 7, and 14 days after both laser treatments. Pattern of cell death on retinal section was evaluated by TUNEL assay, and the distribution of activated inflammatory cells and glial cells were observed under immunohistochemistry. Consecutive changes for the expression of cytokines such as IL-1β, TNF-α, and TGF-β were also examined using immunohistochemistry, and compared among each period after quantification by Western blotting.

Results The numbers of TUNEL-positive cells in the retinal pigment epithelium (RPE) layer did not differ in SRT and cwPC lesions, but TUNEL-positive cells in neural retinas were significantly less on SRT. Vague glial cell activation was observed in SRT-treated lesions. The population of inflammatory cells was also significantly decreased after SRT, and the cells were located in the RPE layer and subretinal space. Proinflammatory cytokines, including IL-1β and TNF-α, showed significantly lower levels after SRT; conversely, the level of TGF-β was similar to the cwPC-treated lesion.

Conclusions SRT resulted in selective RPE damage without collateral thermal injury to the neural retina, and apparently produced negligible glial activation. In addition, SRT showed a markedly less inflammatory response than cwPC, which may have important therapeutic implications for several macular diseases.

Keywords Continuous-wave laser photocoagulation · Inflammatory response · Selective retina therapy · Iba-1 · CD11b · F4/80 · IL-1β · TNF-α · TGF-β

Jung Woo Han and Juhye Choi are co-first authors.

JWH and JC contributed equally to the work presented here and should therefore be regarded as equivalent authors.

✉ Jungmook Lyu
lyujm5@gmail.com

✉ Tae Kwann Park
tkpark@schmc.ac.kr

[1] Department of Ophthalmology, College of Medicine, Soonchunhyang University, Bucheon, South Korea

[2] Department of Medical Science, Konyang University, 158 Gwanjeodong-ro, Seo-gu, Daejeon 320-832, Republic of Korea

[3] Institute of Biomedical Optics, University of Lübeck and Medizinisches Laserzentrum Lübeck GmbH, Lübeck, Germany

[4] Laboratory for Translational Research on Retinal Macular Degeneration, College of Medicine, Soonchunhyang University, Bucheon, South Korea

[5] Department of Ophthalmology, Soonchunhyang University College of Medicine, Soonchunhyang University Bucheon Hospital, #170 Jomaruro, Wonmi-gu, Bucheon-si, Gyeonggi-do 420-767, South Korea

Introduction

Selective retina therapy (SRT) was developed to minimize damage to surrounding tissues by laser therapy and retain its therapeutic effect. SRT selectively damages retinal pigment epithelium (RPE) cells without thermally damaging the neural retina, especially photoreceptors, adjoining the RPE layer or choroid [1]. This selective damage is achieved by the application of microsecond (μs) laser pulses. The delivered pulse energy is primarily absorbed by intracellular melanosomes of RPE cells, and at appropriate energy levels and pulse duration, can selectively damage these cells by microvaporization, which triggers mechanical disruption of the RPE cells. Then, SRT showed therapeutic effect by stimulating RPE cell migration and proliferation into irradiated areas to improve metabolism

at disease-affected locations [2]. Structural restoration and functional preservation following SRT were described in previous studies [3–6]. Hence, SRT has been applied for several macular diseases [7–11].

It has been reported continuous-wave laser photocoagulation (cwPC) induces a train of inflammatory reactions from the death of RPE cells and different types of retinal neurons, of course, mainly, photoreceptors [12–15]. The photothermal and photodisruptive mechanism of RPE damage by cwPC induces cell proliferation not only in the RPE layer itself, but also in the surrounding neural retina and in the underlying choroid and sclera [14]. The responses are characteristic of neuroinflammation, which is triggered primarily by microglia, mediated via release of proinflammatory cytokines, and typically results in exacerbation of primary neuronal damage [14, 16, 17]. To our knowledge, however, the microglia and inflammatory cell responses on chorioretinal tissue including the RPE layer after SRT using 1.7 μs of pulse duration have not been described previously. It would be meaningful to identify the inflammatory cell responses after laser irradiation in the low-μs time domain, rather than the responses after other irradiation times, because it has been known that this laser pulse range could ideally achieve selective RPE targeting [1, 18]. Recently, a study reported cellular responses following the subthreshold laser application using nanosecond laser pulse duration [19, 20]. SRT induces RPE cell death without collateral thermal damage; therefore, the inflammatory responses following SRT will be shown differently from that following laser treatments with cwPC, subthreshold laser photocoagulation or nanosecond laser effects.

In light of the above, we investigated glial cell reactivation and inflammatory responses after SRT using a train of increasing pulse energy with 1.7-μs laser pulses controlled by automated real-time feedback dosimetry in order to apply energy just slightly above RPE cell damage and thus preventing strong mechanical impacts leading to retinal or choroidal disruption. We further compared the neuroinflammatory responses to SRT and cwPC using immunohistochemistry and Western blotting.

Methods

Animals

All mice were handled and experiments performed in accordance with the Association for Research in Vision and Ophthalmology (ARVO) Statement for the Use of Animals in Ophthalmic and Vision Research in order to minimize suffering. The study was approved by the Animal Care Committee of Soonchunhyang University Bucheon Hospital. A total of 76 healthy C57BL/6 J mice were used in this study (OrientBio®, Seongnam, Republic of Korea) at 8 weeks of age. Sixty-six mice were divided into three cohorts. A total of 30 mice (15 for each laser treatment) were used for histology, immunohistochemistry, and terminal deoxynucleotidyl transferase-mediated-dUTP nick-end labeling (TUNEL) assays. The second cohort was comprised of 18 mice (9 for each laser treatment), which were used for retinal whole-mount immunohistochemistry. The third cohort was comprised of 18 mice (9 for each laser treatment), which were used for Western blotting. Ten mice did not receive laser treatment, and served as controls. The mice were kept in a temperature- and humidity-controlled room with a 12:12 h light–dark cycle environment under standardized conditions. Food and water were provided to the mice ad libitum. Prior to laser treatment, all mice were anesthetized with an intraperitoneal (IP) injection of a mixture of Zoletil 50® (125 mg zolazepam and 125 mg tiletamine hydrochloride [Vibrac, Carros, France]; 40 mg/kg of body weight) and Rompun® (2% xylazine hydrochloride [Bayer Animal Health, Leverkusen, Germany]; 5 mg/kg of body weight). Pupil dilation was performed with 0.5% tropicamide and 2.5% phenylephrine (Mydrin-P®; Santen, Osaka, Japan). Only the right eyes of mice were used for laser treatment. The laser treatments and examinations were conducted at the same time of the day.

Laser irradiation

Two kinds of laser modality, SRT and cwPC, were used. The right eyes of mice were treated with SRT (maximal pulse energy: 30 μJ, radiant exposure: 95.5 mJ/cm^2, repetition rate: 100 Hz, pulse duration: 1.7 μs, spot size: 200 μm) performed with the SRT laser system (R-Gen; Lutronic, Goyang, South Korea) using a neodymium-doped yttrium lithium fluoride (Nd:YLF) laser with a wavelength of 527 nm. This laser wavelength is generated from a diode-excited Nd:YLF crystal with intracavity frequency doubling. For each spot, a train of pulses is applied with a frequency of 100 Hz with increasing pulse energy. The first pulse energy is set at 10% of the maximal pulse energy. Then, the energies of consecutive pulsed laser are increased by 3.1% of the maximum pulse energy for each following pulse. Thus, a maximal of 15 pulses are emitted.

It is known that the selective RPE effects are induced by intracellular microbubble formation at the strong absorbing intracellular melanin granula. These short-living microbubbles disrupt the RPE cell membrane owing to the temporally increasing cell volume. In order to prevent extended mechanical damage to the surrounding tissue by

coalescing large microbubbles, a feedback method based on the change of light reflection after bubble formation was developed. The reflectometry detects signals of the back-scattered light, providing an optical feedback value (OFV). For optimizing OFV threshold, we evaluated back-scattered light of the laser irradiation and the pulses were analyzed with a computer equipped with reflectometry algorithms. The "bubble set point" was established when the marked elevation in OFV was detected by reflectometry. Thereafter, the irradiation with pulsed laser was automatically ceased when the OFV reached the preset bubble set point. The methods of SRT application and the determination of the bubble set point were described in detail in our previous study [4, 21].

CwPC (power: 100 mW, duration: 40 ms, spot size: 200 μm, total radiant exposure: 12.6 J/cm^2) was performed with the slit lamp delivery system of a PASCAL Streamline system (Topcon Medical Laser Systems, Inc., Santa Clara, CA, USA) using a frequency-doubled neodymium:yttrium-aluminum-garnet (Nd:YAG) laser diode with a 532-nm wavelength. The right eyes of mice were treated with cwPC. Laser treatment was done in the same manner as SRT.

To neutralize corneal and lenticular diopteric power, a thin transparent hand-held flat glass coverslip was used anterior to the mice eyes as a contact lens with application of 0.5% methylcellulose (Genteal®; Novartis, Basel, Switzerland).

For the morphological studies, such as TUNEL assay and immunohistochemistry, a total of 10 laser lesions were made on the retina, which were distributed in a concentric pattern around the optic nerve head of mouse. When gas bubbles were induced during laser treatment, all of those animals were excluded from the subjects for the current study. For the mice planned to be used for Western blotting, 50 laser spots were induced through the retina in the posterior hemisphere of the eye.

Infrared reflectance imaging and fundus fluorescence angiography

Twelve hours and 1 and 2 days after the laser photocoagulation, infrared reflectance (IR) images and fundus fluorescein angiography (FFA) were taken using a confocal scanning laser ophthalmoscope (Heidelberg Retina Angiograph 2®; Heidelberg Engineering, Heidelberg, Germany). Specifically, animals were anesthetized and pupils were adequately dilated. The IR images were acquired before fluorescein dye injection at each examination period. The angiographic images were captured at 3–5 min after IP injection of 0.1 ml of 2% fluorescein sodium (Fluorescite®; Alcon Laboratories, Inc., Fort Worth, TX, USA) for mice to identify any angiographic visibility of laser-treated lesions over time.

Tissue processing

For tissue preparation, at each time point (12 h, 24 h, 3 days, 7 days and 14 days) after SRT or cwPC, three mice were euthanized for histology. Three mice were also euthanized at each time point (1 day, 3 days, and 7 days) for Western blot analysis. The mice were deeply anesthetized using an IP injection of a 4:1 mixture of Zoletil 50® (80 mg/kg) and Rompun® (10 mg/kg). Thereafter, they were euthanized by intracardial perfusion with 0.1 M phosphate buffer containing 1000 IU/ml of heparin, followed by 4% paraformaldehyde (PFA) in 0.1 M phosphate buffer (PB). After sacrificing the mice, right eyeballs were enucleated and redundant eye tissues were trimmed by scissors. After removal of the anterior segment and lens by cutting through the limbal cornea, the eyecups were immersed in fixative solution composed of 4% paraformaldehyde in 0.1 M PB for fixation at 4 °C and pH 7.4 for 1 h. Nictitating membrane remained attached to the nasal side of the limbus in order to determine the specimen orientation. Then, the samples were transferred to 30% sucrose in phosphate buffer solution (PBS), incubated overnight, and embedded in optimum cutting temperature (O.C.T.) compound (Sakura Finetek, Torrance, CA, USA). The serial sagittal sections (in the 12–6 o'clock plane) with thicknesses of 8 μm were taken from the embedded samples, and mounted on adhesive microscope slides (Histobond®; Paul Marienfeld GmbH & Co. KG, Lauda-Königshofen, Germany). By visually scanning all the serial section, the transverse chorioretinal sections with the furthest disruption at the RPE-photoreceptor junction were designated as the center of the laser lesion. For retinal whole-mount immunohistochemistry, laser-treated eyes were dissected into posterior eyecups. After peeling of the neural retina, RPE-choroid complexes were fixed in 4% PFA, and prepared as flattened whole-mounts with four quadrants cuts.

Immunohistochemistry

Immunohistochemistry on the chorioretinal sections of the mice retina was performed to identify glial cell activation and expression of the cytokines after SRT and cwPC. The antibodies used for immunohistochemistry in the current study are described in Table 1. Reactivity of Müller cells was determined by the expression of glial fibrillary acidic protein (GFAP) at seven days after cwPC or SRT treatment. The integrity of cell-to-cell junction and hexagonality of the RPE layer were evaluated by labeling with β-catenin. Antibodies for ionized calcium-binding adaptor molecule-1 (Iba1), CD11b, and F4/80 were used to confirm the cell identity of retinal microglia, monocyte, and macrophage in the chorioretinal sections, respectively.

Table 1 Antibodies used for immunohistochemistry and Western blot in the current study

Target	Host	Manufacturer	Catalog no.	Dilution
GFAP	Rabbit	Millipore, Billerica, MA, USA	AB5804	1:1000
iba1	Rabbit	Wako Chemicals, Osaka, Japan	#019–19,741	1:1000
CD11b	Rat	Serotec, Oxford, UK	MCA711G	1:2000
F4/80	Rat	Serotec, Oxford, UK	MCA497GA	1:2000
IL-1β	Mouse	Cell Signaling Technology, Danvers, MA, USA	#12242	1:1000
TNFα	Rabbit	Abcam PLC, Cambridge, UK	Ab66579	1:2000
TGFβ	Rabbit	Abcam PLC, Cambridge, UK	Ab66043	1:2000

The vertically sectioned images from chorioretinal preparation were acquired using a fluorescence microscope (AxioPlan®Fluorescence Microscope; Carl Zeiss Inc., Oberkochen, Germany) with ×200 magnification and 1.5-s exposure. The taken images were digitalized with a monochromatic charged-coupled device (CCD) camera (AxioCam MRm®, Carl Zeiss Inc., Oberkochen, Germany). Each chorioretinal section image was captured by image-capture software (AxioVision® LE 4.8.2; Carl Zeiss Inc., Oberkochen, Germany). The images from whole-mount preparation were obtained using confocal fluorescence microscopy (LSM510 META®, Carl Zeiss Inc., Oberkochen, Germany). The images were taken using image-capture software (LSM® image browser, Carl Zeiss Inc. Oberkochen, Germany) with ×200 magnification for whole mounts.

For staining cell markers, the slides were incubated with antibodies for each cell marker at 37 °C for 2 h. Detection of the signal was achieved by incubation with the appropriate combination of AlexaFluor 488 and AlexaFluor 568 conjugated secondary antibodies, and 4′,6-diamidino-2-phenylindole dihydrochloride (DAPI, 0.1 μg/ml, Sigma-Aldrich, St. Louis, MO, USA) stain was used for labeling the cell nuclei with 3 min of incubation time. The other samples were treated with the same methods as described above. Subsequently, they were mounted and examined under an Axioplan® microscope and LSM510® confocal fluorescence microscope for chorioretinal section images and whole-mount images, respectively.

TUNEL assay

The in situ Cell Death Detection Kit, Fluorescein® (Roche Diagnostics, Basel, Switzerland) was used for TUNEL assay of the current study to detect the cell death after laser treatments with SRT and cwPC. TUNEL assay was carried out 24 h after laser treatments, according to the protocols recommended by the kit manufacturer. The briefly summarized procedures are described as follows. The chorioretinal preparation was washed with PBS for 10 min, and repeated 3 times. The sample was incubated with blocking solution of 3% H_2O_2 in methanol for 10 min at 15 to 25 °C. Repeated washings were performed three times with PBS. Then, the sample was incubated in permeabilisation solution consisting of 0.1% Triton X-100 and 0.1% sodium citrate (Sigma-Aldrich, St. Louis, MO, USA) for 2 min on ice (2 to 8 °C). After tissue washings with PBS, labelling reaction was achieved using a TUNEL reaction mixture. The chorioretinal section was evaluated under the fluorescence microscope, after incubation at 37 °C for 60 min.

Western blotting

Expressions of the cytokines including IL-1b, TNF-α, and TGF-β following SRT and cwPC were analyzed by Western blotting of chorioretinal extracts. Following sacrifice of mice, the cornea and the lens of the eyeballs were removed after enucleation, and 80 μl of lysis buffer was added. Tissue extracts from the mice eyes were sonicated, then they were placed on the ice for 50 min. Hence, the extracts were centrifuged at 4 °C for 20 min at 12,000 rpm. After centrifuging, the supernatants were collected, and the protein concentration in the homogenate was measured using the commercial protein assay kit (Pierce®BCA Protein Assay Reagent Kit; Thermo Scientific, Rockford, IL, USA) according to the protocols recommended by the manufacturer. An equal volume (20 μg) of total protein from each extract was resolved on sodium dodecyl sulfate (SDS) polyacrylamide gel electrophoresis, and then the proteins were transferred to a nitrocellulose membrane. The membranes were blocked by 5% skim milk for 1 h at room temperature and incubated with the appropriate antisera overnight at 4 °C (Table 1). Consequently, the membrane was incubated again with goat anti-rabbit or goat anti-mouse horseradish peroxidase-conjugated secondary antibodies (1:5000, Santa Cruz Biotechnology, Inc. Dallas, TX, USA) for 90 min at room temperature. The blot was developed by the enhanced chemiluminescence system (Clarity® ECL Western Blotting Substrate; Bio-Rad Laboratories Inc. Hercules, CA, USA). The positive labeling band was detected, and densitometry of the band was performed by drawing the bands of interest. The quantification of detected bands was achieved using Image J® software (National Institute of Health, Bethesda, MD, USA). Detection of β-actin was assessed in all samples as a positive gel-loading control.

Cell counting

The number of TUNEL-positive cells was estimated on chorioretinal sections to quantify the apoptotic cells, because the TUNEL labeling represents the cellular apoptosis of the whole laser-treated lesion. The TUNEL-positive cells were manually counted by three independent experienced colleagues who were unaware of the treatment performed on each specimen. Cell counting was done separately for two different layers such as the neural retina and the RPE. Five laser-treated lesions showing typical morphology were selected and averaged from each animal for the quantitative analysis. In addition, quantification of labeled cells on whole-mount views after SRT and cwPC was performed by the measurement of the labeled area. The area showing immunoreactivity in the entire microscopic field was quantified using Image J®. All quantified values were given as mean ± standard error of the mean (SEM).

Statistical analysis

Statistical analysis was performed using the SPSS software (version 20.0 for Windows, SPSS Inc., Chicago, IL, USA). The two-tailed Student's *t* test was used to compare the results of the cell counting after the immunohistochemistry for cytokines following two laser treatments between SRT and cwPC at each examination period. The number of the cells labeled TUNEL-positive were also compared between two laser treatments using Student's *t* test. A probability value of 0.05 was considered to indicate statistical significance for the Student's *t* test. In addition, quantified results of Western blotting after SRT and cwP were averaged using three samples, and the results at each time were compared with the expression level of the control. Bonferroni correction was used for multiple comparison among examination periods in order to reduce the alpha error. A probability value of 0.0125 was applied for statistical significance after Bonferroni correction.

Results

Infrared and FFA findings

Laser burns could be identified in vivo using IR imaging immediately and consecutive FFA after 1 day following SRT and cwPC (Fig. 1A–C, E–G). At 2 days after SRT, the FFA image did not reveal any hyper-fluorescences in the previously visible laser spots (Fig. 1D). Following cwPC, however, hyper-fluorescences were observed at 2 days (Fig. 1H).

Time-dependent changes in the RPE at the laser-treated area

To evaluate the consecutive structural changes in RPE cells after the treatments, the expression patterns of β-catenin, a component of cell–cell connections, were observed at 1, 3, and 7 days following SRT and cwPC treatment. At baseline, β-catenin delineates the contours of each RPE cell, revealing their hexagonal shape. At 24 h after treatment, β-catenin was not detected at the center of the SRT spot and the contours of the surrounding RPE cells were elongated centripetally. Expression from the membranous portion of the elongated RPE cells was more aberrant, which might have resulted from the loosening of cell–cell connections (Fig. 2A). At 3 days later, the center of the SRT lesion was covered with RPE cells and cell–cell connections (Fig. 2B). The hexagonality of RPE cells was almost restored at 1 week after treatment (Fig. 2C).

Beta-catenin expression was different in cwPC-treated lesions. At 24 h, β-catenin was not detected at the center of the cwPC-treated lesions and extended damage to RPE integrity was identified (Fig. 2D). After 3 days, the center of the cwPC-treated lesion was gradually covered with RPE cells via elongation, but the membranous portion of the elongated RPE cells was aberrant and the hexagonal shape was not restored (Fig. 2E). After 7 days, the cell–cell connections and hexagonal shape of RPE cells were partially restored. (Fig. 2F).

Cell death assay

To determine which cell types were affected by SRT and cwPC treatment, the TUNEL assay was performed 1 day after each treatment. TUNEL-positive cells were clearly detected in the RPE layer of SRT-treated eyes. In a Nomarski view from the same section, waveform discontinuity and irregularity of the RPE layer were also notified. However, in the outer nuclear layer (ONL) of the neural retina, TUNEL-positive cells were not detected (Figs. 3A–C). Conversely, TUNEL-positive cells were abundant not only in the RPE layer but also in the ONL of cwPC-treated eyes (Fig. 3D, E). To quantify the amount of apoptotic cell death after the two treatments, the numbers of TUNEL-positive cells detected in the RPE layer and neural retina of the central transverse sections were assessed, because those cells represent the number of apoptotic cells in the entire laser lesion. The number of TUNEL-positive cells in the RPE layer of SRT-treated eyes was 10, and that in the RPE layer of cwPC-treated eyes was 10 ($p > 0.5$). Thus, there were no significant differences between the groups. However, the numbers of TUNEL-positive cells in the neural retina (detected mostly in the ONL) differed significantly between the two treated arms. In SRT-treated eyes, TUNEL-positive cells were very rare in the ONL; however, such cells were heavily

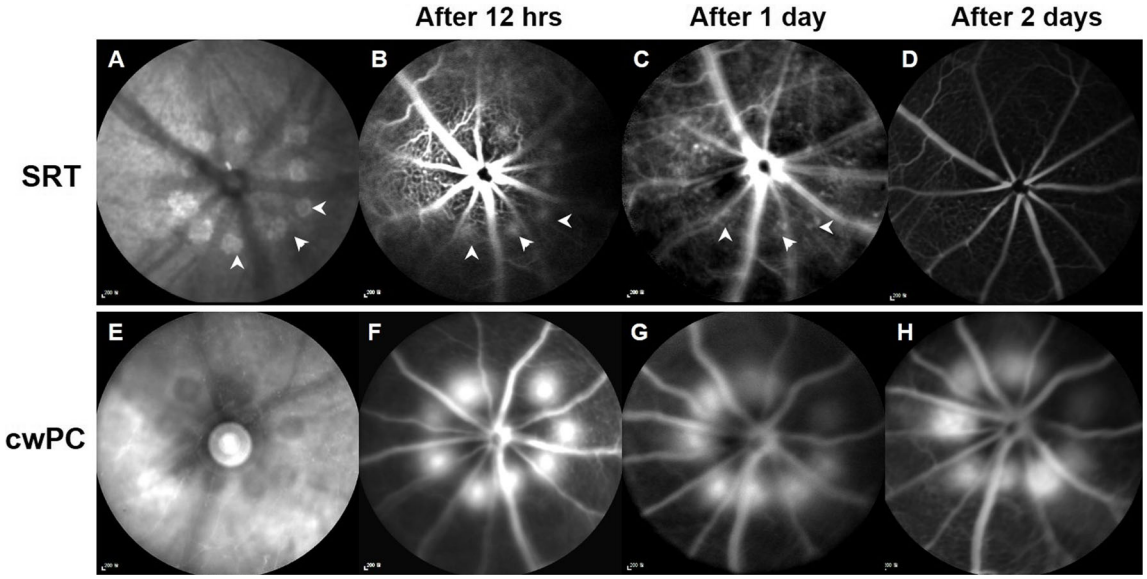

Fig. 1 Initial infrared reflectance images and consecutive findings of fundus fluorescein angiography following selective retina therapy (SRT) and continuous-wave laser photocoagulation for 2 days. Hyperfluorescent spots were observed until 1 day after SRT (**B, C**; arrowheads), but the hyperfluorescence was no longer identified at that point (**D**). By contrast, cwPC-treated lesions showed hyperfluorescence continuously for 2 days after laser irradiation (**E** to **H**)

detected in the ONL of cwPC-treated eyes ($p < 0.01$; $2 \pm a$ in the SRT arm vs. $120 \pm b$ in the cwPC arm).

Glial cell responses after treatment

Immunolabeling for GFAP was performed to evaluate reactive hypergliosis after SRT and cwPC treatment. GFAP expression was detected weakly only in the Müller cell end feet and the inner half of the neural retina 7 days after SRT treatment. To confirm the exact location of the SRT-treated area, Nomarski images were taken simultaneously, and showed irregular discontinuities in the RPE layer (Fig. 4A–C). However, in cwPC-treated eyes, GFAP expression was clearly distributed throughout the whole layer of the neural retina, and particularly in the ONL of the center of the treated spot, that is, the area in which the photoreceptor cells were most severely affected; this was detected most strongly at 7 days after treatment (Fig. 4D, E).

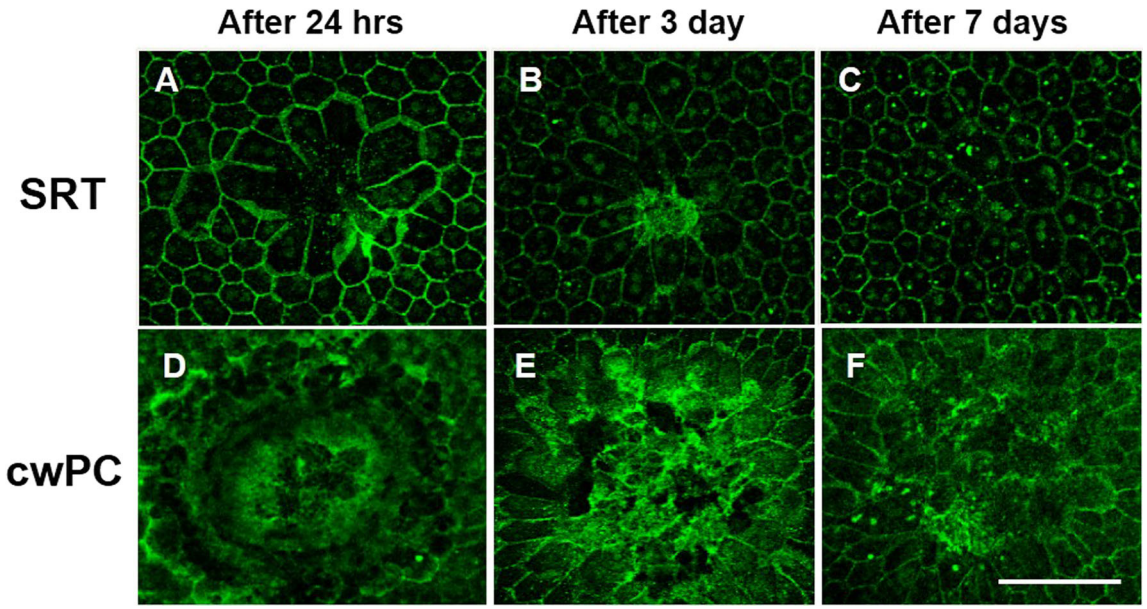

Fig. 2 Consecutive images of immunostaining with β-catenin following SRT and cwPC. Elongation of the hexagonal structure in the RPE layer was observed after SRT; then it was almost restored at 7 days (**A** to **C**). However, extended damage to RPE integrity, which did not recover a normal hexagonal structure, was identified in cwPC-treated lesions (**D** to **F**)

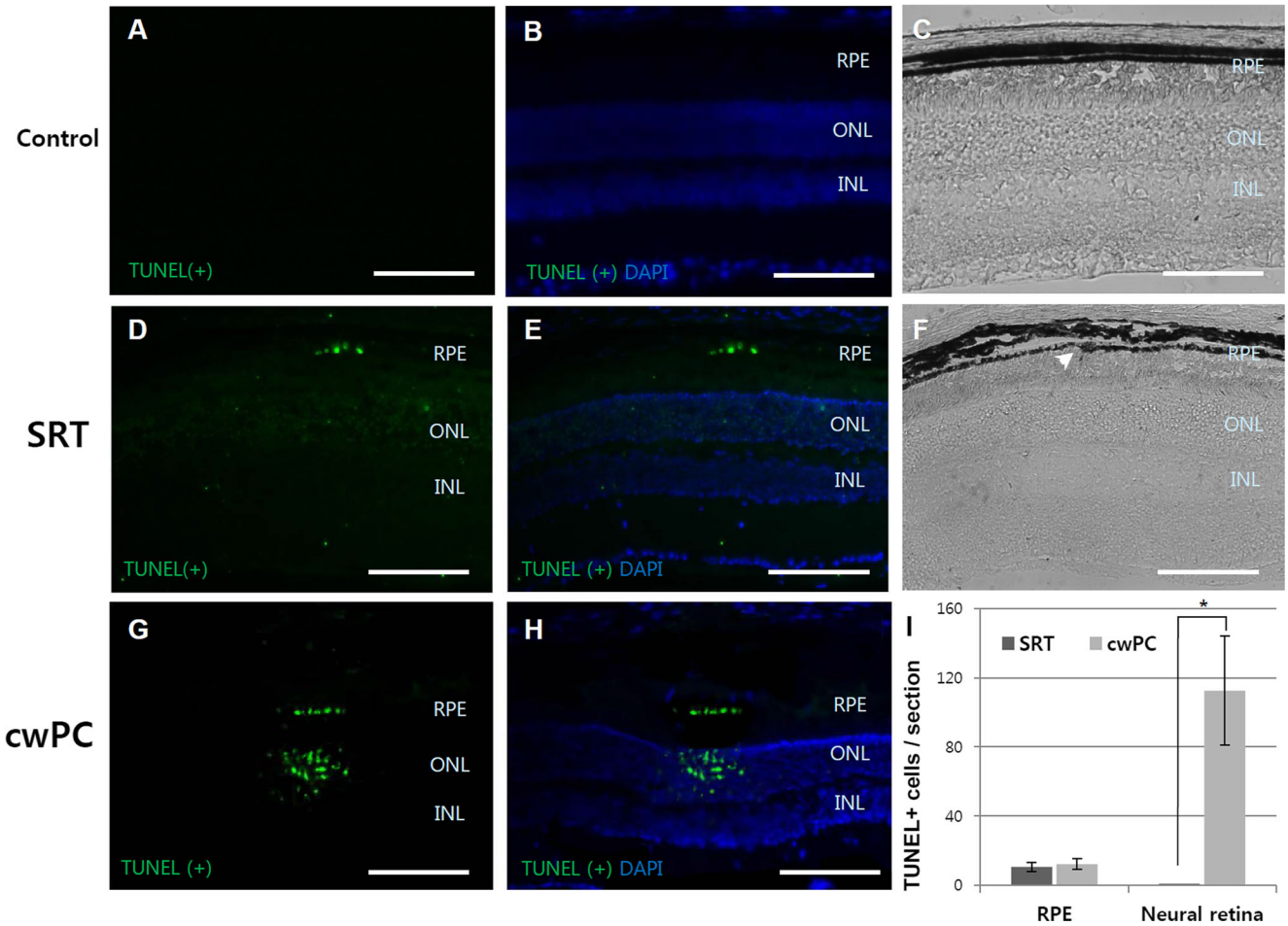

Fig. 3 Representative images of cell death at 1 day following the laser treatments with SRT and cwPC. In the control group, TUNEL-positive cells were not seen in the RPE and neural retina. (**A, B**) In an SRT-treated lesion (**F**, arrowheads), TUNEL-positive cells were observed in the RPE layer, while they sporadically appeared in the neural retina (**D, E**). In a cwPC-treated lesion, cell deaths labeled by TUNEL were identified on the RPE and neural retina (**G, H**). Quantification of TUNEL labeling at 1 day after SRT and cwPC (*I*). The number of TUNEL-positive cells shown in the RPE layer was not significantly different between SRT- and cwPC-treated lesions. On the other hand, the number of TUNEL-positive cells detected in the neural retina was significantly higher in cwPC-treated lesions than SRT-treated lesion (**I**). Data was expressed as the mean ± SEM. $n = 3$ mice per group $^*P < 0.01$ by Student's t test. Scale bar = 100 μm

Recruitment and infiltration of inflammatory cells

To detect recruitment and accumulation of leukocyte populations after SRT and cwPC, we performed immunolabeling for iba1, F4/80, and CD11b, which are well-characterized markers for microglia, macrophages, and monocytes, respectively. In unlasered control eyes, microglia were found with branched processes in the outer plexiform layer (OPL) and inner plexiform layer (IPL), while macrophages and monocytes were found in the OPL, IPL, and choroid as evidenced by immunolabeling of retinal transverse sections (Figs. 5A–C). At 7 days after SRT, the expressions of iba1, F4/80, and CD11b in the OPL and IPL were similar with those in unlasered control eyes. The number of inflammatory cells with up-regulated immunoreactivity and amoeboid shape was relatively increased in the RPE layer and subretinal space (Fig. 5D–F). Following cwPC, however, intense expressions of iba1, F4/80, and CD11b were featured in almost all retinal layers from the IPL to subretinal space at 7 days, indicating that inflammatory cells undergo a proliferative phase (Fig. 5G–I). The number of labeled inflammatory cells noticeably increased, and they revealed an amoeboid morphology with few processes. In addition, the expression of Iba1 and CD11b were sustained at a similar level from 12 h to 14 days at the center of the SRT lesion (Fig. 7A–F).

Unlasered control eyes did not display any immunoreactivity, as evidenced by immunolabeling of retinal whole-mounts (Fig. 6A, E, I). Following SRT, markedly less localized cells were found compared with cwPC (Fig. 6B, C, F, G, J, K). Quantification of iba1, F4/80, and CD11b using the measurement of the labeled area showed that the labeled area after cwPC-treated lesions were significantly higher than SRT-treated lesions ($p < 0.05$) (Fig. 6D, H, L).

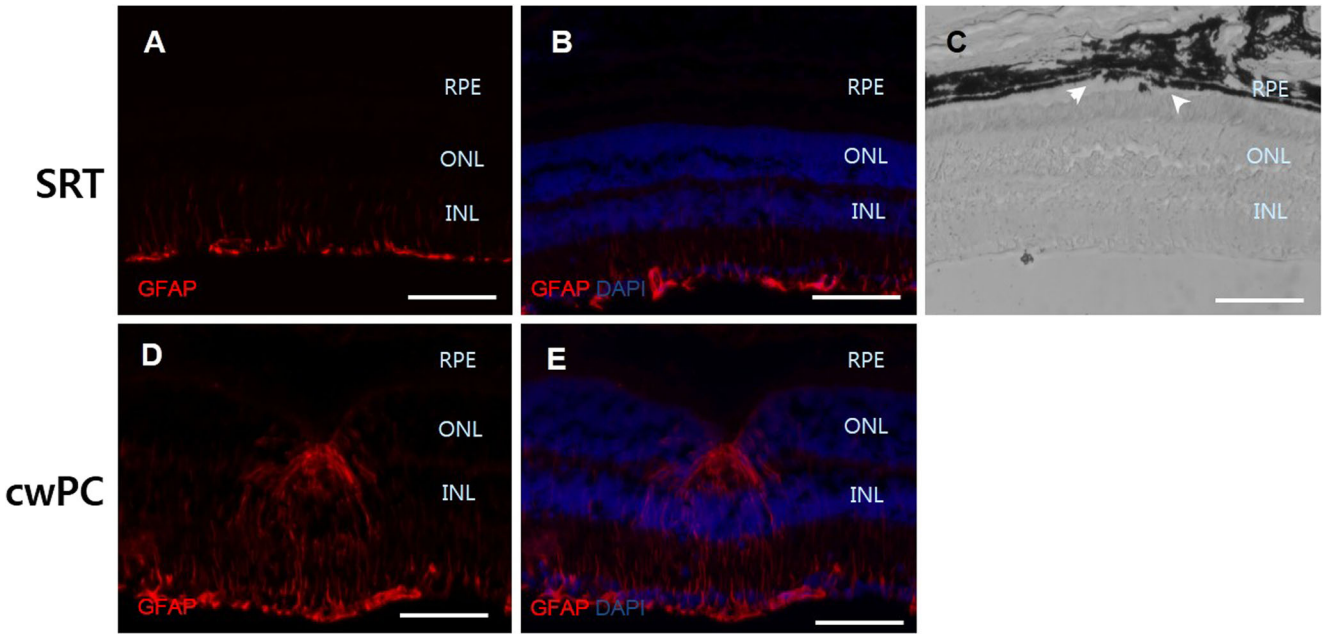

Fig. 4 Expression of GFAP following laser treatments with SRT and cwPC. Representative images of chorioretinal sections with GFAP immunostaining at 7 days after laser irradiation. Expression of GFAP in the SRT-treated lesion (**C**, arrowheads) was vaguely identified and limited to the inner retina (**A, B**), whereas intensely GFAP-labeled cells were evident in the whole retinal layer in the cwPC-treated lesion (**D, E**). Scale bar = 100 μm

Time-dependent changes in proinflammatory cytokines and TGF-β

To investigate the change in expression of proinflammatory gene products after SRT and cwPC, we performed Western blotting and the quantification of the expressions of IL-1β, TNF-α, and TGF-β. Following SRT, IL-1β expression was increased at 1 day, then declined after 3 days. By 3 days after cwPC, IL-1β expression was decreased, and significantly increased at 7 days (Fig. 8A, B). The patterns of expression of TNF-α after two laser treatments were broadly similar to those of IL-1β. TNF-α expression was significantly increased at 1 and 3 days after cwPC (Figs. 8A, C). Meanwhile, TGF-β expression was significantly increased at 1 and 3 days after SRT and cwPC, and the increments of TGF-β expression from the control were similar in two laser treatments, unlikely to the results of IL-1β and TNF-α (Fig. 8A, D).

Discussion

Laser photocoagulation has been the management choice of clinicians for decades in the treatment of several macular diseases. After laser photocoagulation, inflammatory responses are induced according to cell death by thermal injury in retinal tissue. When a laser is applied, the Müller cells located directly at the burn site become reactive, with increasing expression of the intermediate filament protein GFAP [22]. The stimulation of inflammatory cells in response to retinal tissue injury causes the release of cytokines such as IL-1β, IL-3, IL-6, and TNF-α to propagate an inflammatory response within the retina, leading to increased inflammatory cell infiltration [12]. A previous study demonstrated that laser photocoagulation induced the proliferation of various kinds of cells, including inflammatory cells, RPE cells, endothelial cells, and Müller cells [23]. These inflammatory responses would be therapeutically necessary as a wound-repair process following laser photocoagulation. In addition, the proliferation and migration of RPE cells to a disease-affected location can be stimulated by laser treatment [31]. However, excessive glial and fibrotic changes in retinal tissue or laser-induced macular edema can result in inflammatory responses after laser treatment [24, 25].

SRT with automated real-time feedback dosimetry provides a therapeutic modality that can confine cell damage to the RPE layer and guarantee that irradiation is within the safe range of the therapeutic window. Thus, selective damage to the RPE is possible without collateral damage to the overlying neural retina and underlying choroidea [1, 2]. Over the past decade, studies have applied SRT to treat geographic atrophy, diabetic macular edema (DME), central serous chorioretinopathy (CSC), and persistent subfoveal fluid accumulation after rhegmatogenous retinal detachment [7–11]. In the present study, the inflammatory and glial responses of mice were evaluated and compared between mice treated with cwPC and those treated with SRT.

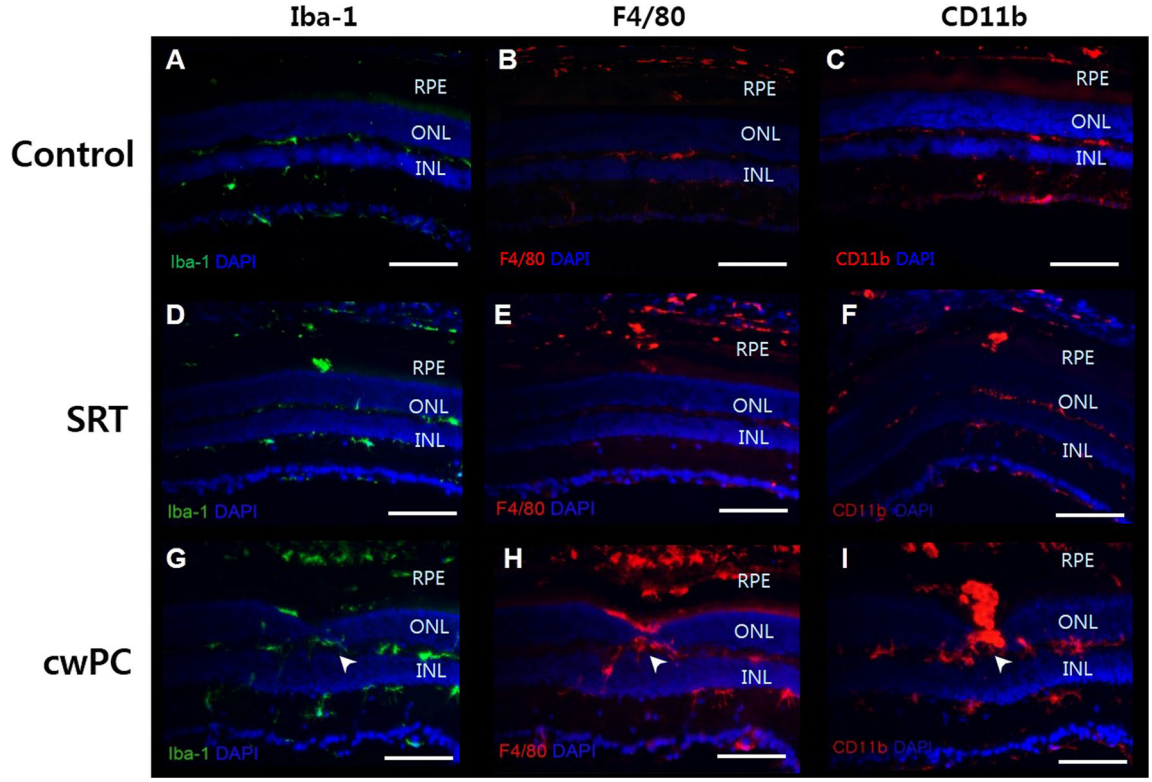

Fig. 5 Inflammatory cells following laser treatments with SRT and cwPC. Representative images of chorioretinal sections labeled with Iba1, F4/80, and CD11b at 7 days after laser treatments. In the resting state, expression of Iba1 (**A**) was seen in branched processes in the OPL and IPL. Expression of CD11b (**B**) and F4/80 (**C**) was observed in the OPL, IPL, and choroid before laser treatments. After SRT irradiation, expression of Iba1 (**D**), CD11b (*E*), and F4/80 (**F**) in the OPL and IPL was similar to the resting state, while the numbers of inflammatory cells with upregulated immunoreactivity and amoeboid shapes were increased in the RPE layer and subretinal space (**D–F**, arrows). In cwPC-treated lesions, however, intense expression of Iba1 (**G**), F4/80 (H), and CD11b (**I**) was seen in almost all retinal layers, from the IPL to the subretinal space. In addition, the number of labeled inflammatory cells increased noticeably, and they revealed amoeboid morphologies with few processes (**G** to **I**, arrowheads). Scale bar = 100 μm

SRT resulted in hyperfluorescent spots on FFA, but the hyperfluorescence disappeared after 1 day. In addition, the loss of hexagonality in the RPE layer that occurred with SRT was apparently restored at 7 days, unlike in cwPC lesions. Cell death following SRT was not identified in the neural retina, but was limited to the RPE layer. Glial cell activation in SRT lesions was also markedly less than in cwPC-treated lesions. According to the results of immunohistochemistry, increased reactivity and the recruitment of inflammatory cells were observed within the SRT-treated lesion, which maintained revelation for 12 h and for up to 14 days after SRT treatment. However, the population of inflammatory cells was significantly smaller than in cwPC lesions and they were located in the RPE layer and subretinal space. These findings suggest that phagocytosis of RPE debris resulted from SRT application.

Using Western blot analysis, the expression of proinflammatory cytokines, including IL-1β and TNF-α, was estimated. The IL-1 family plays a key role in the initiation of acute inflammatory responses. IL-1β can be secreted by RPE cells and is a potent inflammatory mediator with chemotactic and angiogenic properties [24, 26, 27]. Thus, IL-1β expression increases rapidly in laser-induced injury to the retina [18]. In the present study, the expression of IL-1β in SRT-treated lesions increased and then declined. However, significantly increased expression of IL-1β was evident at 7 days after cwPC. Thus, SRT induced a slight increase in IL-1β temporarily for a few days, when compared to cwPC. Additionally, the expression of TNF-α after SRT was significantly decreased after 1 and 3 days compared with cwPC. TNF-α is a secreted proinflammatory cytokine that plays a role in cellular proliferation, has chemotactic effects on inflammatory cells, and participates in distinct angiogenesis-related processes in the retina [28–30]. Generally, TNF-α levels are elevated significantly after laser photocoagulation in the retina [30]. In the present study, the immunoreactivities of TNF-α were elevated after SRT and cwPC. In particular, the immunoreactivities on cwPC-treated lesions were increased significantly at 1 and 3 days versus control levels compared to the increases on SRT-treated lesions. These findings suggest that less expression of TNF-α is induced by SRT than by cwPC. In addition, the migration and recruitment of inflammatory cells, shown by immunohistochemistry (Fig. 5), were

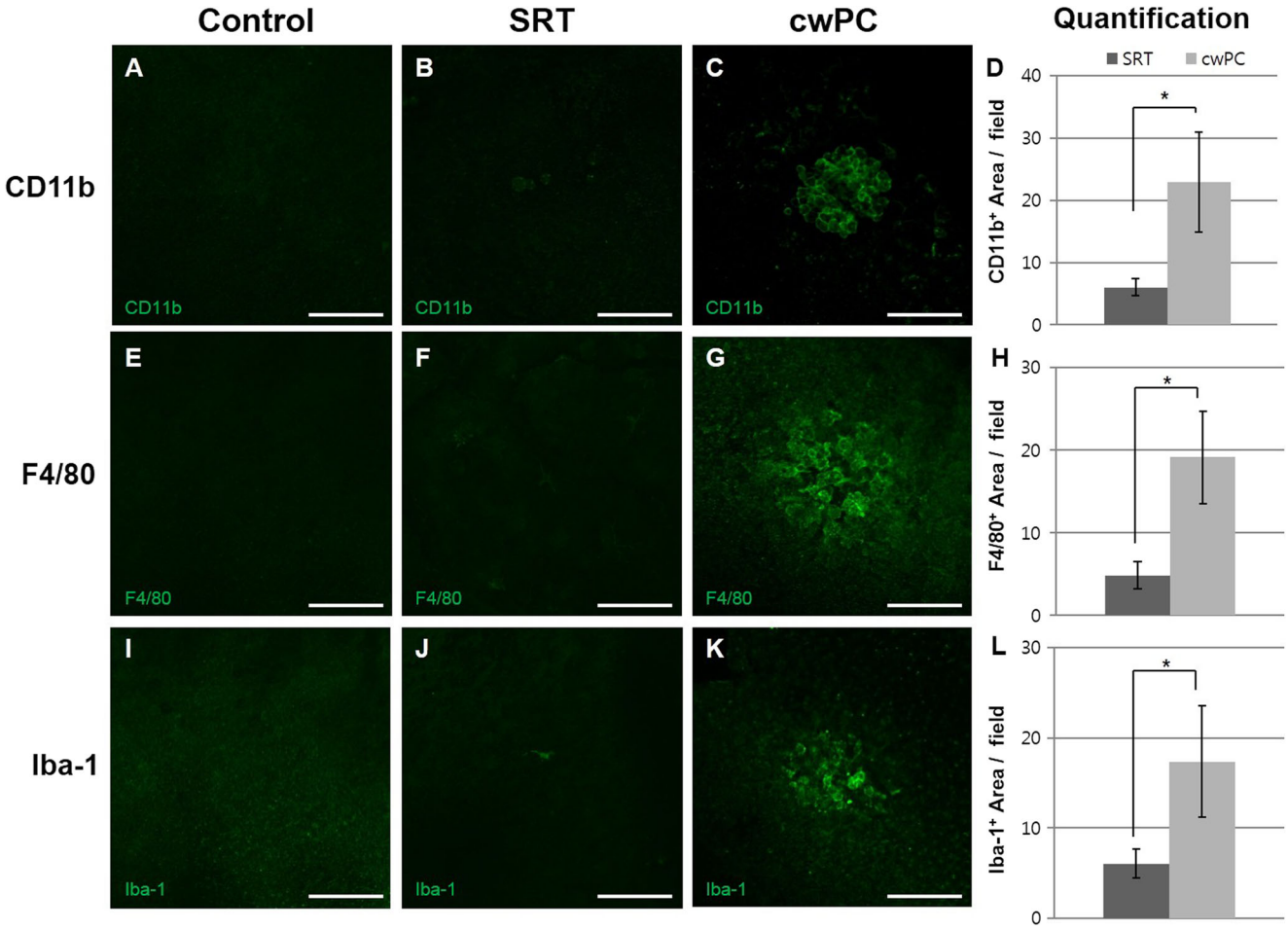

Fig. 6 Levels of inflammatory cells following laser irradiation in SRT and cwPC. Representative images of whole-mount preparations stained with Iba1, F4/80, and CD11b at 7 days after laser treatment. SRT-treated lesions (**B, F**, and **J**) demonstrated markedly fewer localized cells than cwPC-treated lesions (**C, G**, and **K**), respectively. The mean fluorescence intensity was calculated using ImageJ software for Iba1-, F4/80-, and CD11b-labeled cells after SRT and cwPC in the labeled areas (**D, H**, and **L**). The labeled areas after cwPC treatment were significantly higher than in SRT-treated lesions (**D, H**, and **L**). All data are expressed as means ± SEM. $n = 3$ mice per group, $^*P < 0.05$, according to the Student's t test. Scale bar = 100 μm

associated with the increased expression of proinflammatory cytokines such as IL-1β and TNF-α.

The levels of TGF-β were similar to those in cwPC lesions, unlike the proinflammatory cytokines mentioned above. Members of the TGF-β superfamily are multifunctional cytokines that regulate several cellular processes, including cell cycle arrest, differentiation, morphogenesis, and apoptosis. TGF-β is a major inducer of the epithelial mesenchymal transition (EMT) during development and fibrotic disease [31]. Intraocular TGF-β2 levels increase significantly following cwPC, and TGF-β plays an important role in chorioretinal wound healing [32, 33]. TGF-β is known to inhibit vascular endothelial cell proliferation induced by fibroblast growth factor (FGF), and it has inhibitory effects on DNA synthesis and chemotaxis [33, 34]. In the present study, the levels of TGF-β were increased at 1 day after both laser treatments. Immunoreactivity for TGF-β at 1 and 3 days showed similar levels in SRT- and cwPC-treated lesions (Fig. 7). As a result, we found that the subsequent expression of TGF-β involved in the EMT was no different using SRT versus cwPC. We also showed that the expression of IL-1β and TNF-α, which are regarded as potent inflammatory mediators, were significantly reduced using SRT. These results show that SRT, unlike cwPC, induces a low-level inflammatory response and provides a positive effect that increases the expression of TGF-β involved in wound healing. Thus, SRT might induce RPE proliferation through the EMT, accompanied by a low-level inflammatory response. Significantly elevated levels of inflammatory cytokines were identified after cwPC, and cwPC sometimes results in decreased visual acuity because of laser-induced macular edema, resulting from inflammatory responses [25, 35–37]. Therefore, we suggest that the risk of laser-induced macular edema might be reduced in SRT-treated eyes compared to cwPC-treated eyes (Fig. 8).

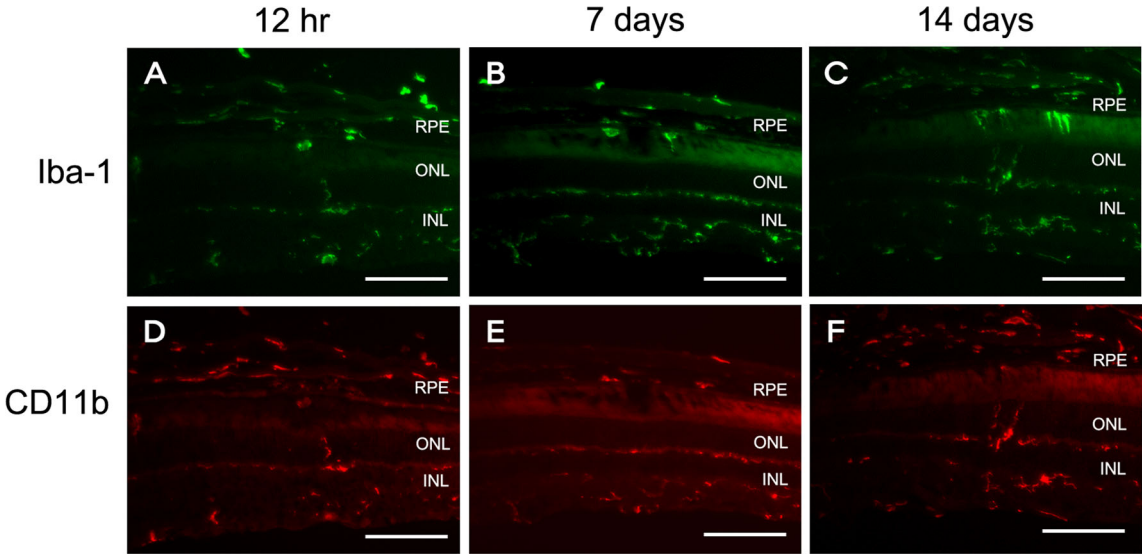

Fig. 7 Consecutive changes in the levels of inflammatory cells following SRT treatments. At 12 h after SRT treatment, the expression of Iba1 (**A**), and CD11b (**D**) was seen in the OPL, IPL, and choroid. In addition, the numbers of inflammatory cells were increased in the RPE layer and subretinal space. At 7 and 14 days after SRT treatment, the expression of Iba1 (**B, C**), and CD11b (**E, F**) from the IPL to the subretinal space were sustained at a similar level. Scale bar = 100 μm

Several studies that performed laser photocoagulation using short-pulse lasers showed that it caused less inflammation in retinal tissue. Laser photocoagulation using various short pulses from microsecond to nanosecond lasers has been previously tried. Significantly fewer infiltrating inflammatory cells and lower expression levels of proinflammatory cytokines were identified in short-pulse laser photocoagulation with a duration of 20 milliseconds, compared to

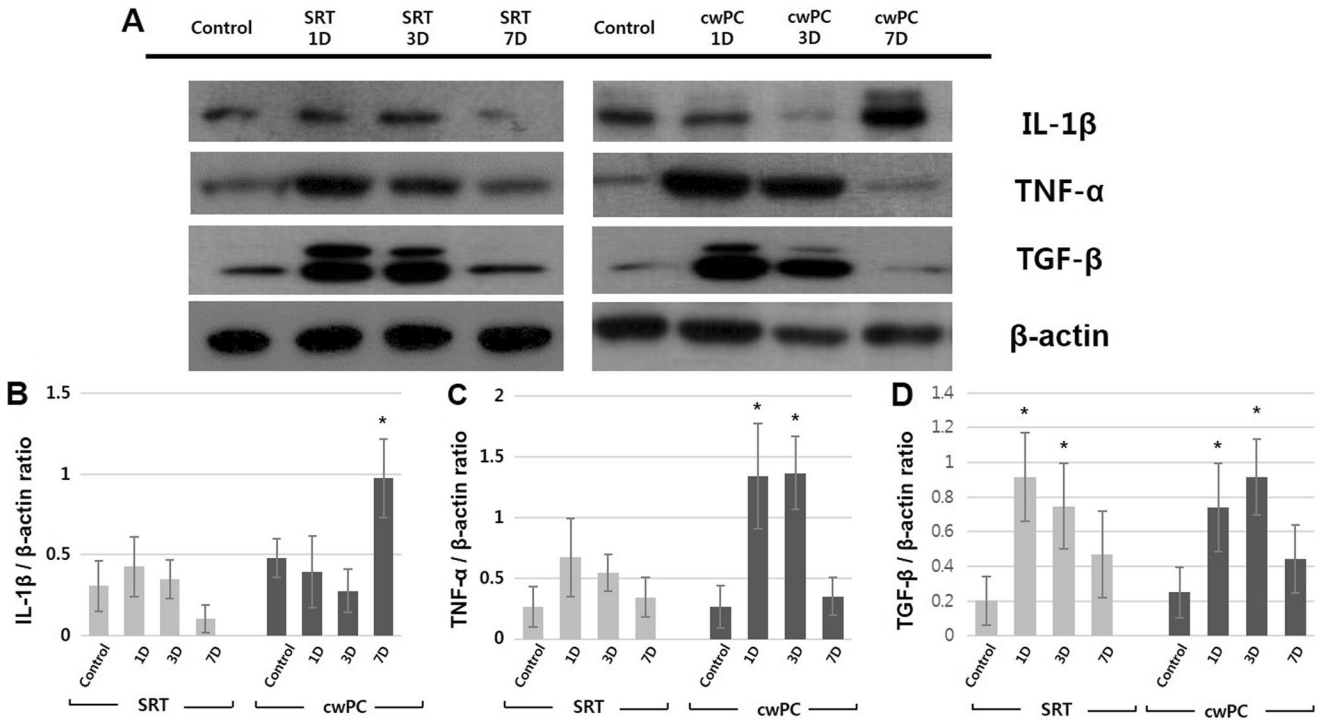

Fig. 8 Consecutive changes in the levels of cytokines, including IL-1β, TNF-α, and TGF-β, following SRT and cwPC laser treatments. Western blot (**A**) and the quantification of the levels of cytokines (**B–D**). Expression of IL-1β was significantly greater at 7 days after cwPC than SRT (**B**). Levels of TNF-α were also increased significantly after cwPC for 3 days (**C**). Levels of TGF-β were increased significantly at 1 and 3 days after SRT and cwPC, and the increments in TGF-β expression versus the control were similar with the two laser treatments, unlike the results of IL-1β and TNF-α (**D**). Data are expressed as the ratio between the expression of cytokines and β-actin. n = 3 mice per group $*P < 0.0125$, according to the Student's *t* test with Bonferroni's correction

conventional laser photocoagulation with a duration of 100 milliseconds [35]. In another study, the so-called retinal regeneration (2RT) laser with a duration of 3 ns was used. It showed selective damage to RPE cells while limiting collateral photoreceptor damage compared with conventional laser photocoagulation [19]. Jobling et al [38] recently performed immunohistochemical analyses of humans and mice after receiving a single 3-ns laser treatment, and found that the retinal structure was not compromised in either human or mouse retina, and only discrete RPE injury was observed. However, a limited mononuclear cell response was observed.

Nanosecond lasers show additional nonlinear damage mechanisms (not just microbubble formation), which are included in laser-induced cellular breakdown or shockwave effects [20, 39, 40]. Laser treatment with nanosecond duration resulted in relatively intense thermomechanical damage to the RPE with the risk of neuroretinal and choroidal disruption, possibly followed by visual impairment and bleeding [2, 39, 40]. Using microsecond durations, microbubble sizes are intrinsically limited in size over a large range of pulse energies, and it is unlikely that nanosecond laser irradiation results in a linear increase in bubble size with pulse energy [39]. With the addition of a bubble detection feedback algorithm, SRT becomes a very selective and safe treatment option, suitable for macular laser applications, even in the foveal area.

In conclusion, SRT caused selective RPE damage without collateral thermal injury to the neural retina, and it induced mild glial cell activation. A smaller population of inflammatory cells were observed in retinal tissue after SRT than in cwPC lesions. Inflammatory cells were limited to the RPE layer and subretinal space, and significantly less expression of proinflammatory cytokines was identified in SRT lesions 7 days after treatment. However, the levels of TGF-β, unlike those of proinflammatory cytokines, were similar to the levels in cwPC lesions. SRT demonstrated a significantly lower inflammatory response than cwPC, suggesting that the risk of laser-induced macular edema and the formation of scar tissue would be lower after SRT than after cwPC. In addition, RPE proliferation through EMT stimulation might be achieved by SRT. Recently, there have been studies to treat retinal diseases such as DME and central serous retinopathy (CSR) using SRT, but SRT has not been widely used clinically for the treatment of retinal diseases. Therefore, further research on the response of RPE cells following SRT and the efficacy of SRT for the treatment of retinal diseases should be performed.

Funding This research was supported by a grant from the Korea Health Technology R&D Project through the Korea Health Industry Development Institute (KHIDI), funded by the Ministry of Health and Welfare (grant number: H I 17C0966, TK Park). This work was partially supported by the Soonchunhyang University Research Fund. The sponsor had no role in the design or conduct of this research.

Compliance with ethical standards

Conflict of interests All authors certify that they have no affiliations with or involvement in any organization or entity with any financial interest (such as honoraria; educational grants; participation in speakers' bureaus; membership, employment, consultancies, stock ownership, or other equity interest; and expert testimony or patent-licensing arrangements), or non-financial interest (such as personal or professional relationships, affiliations, knowledge or beliefs) in the subject matter or materials discussed in this manuscript.

Animal experiments All applicable international, national, and institutional guidelines for the care and use of animals were followed. All procedures performed in studies involving animals were in accordance with the ethical standards of the institution at which the studies were conducted.

Financial disclosure None of the authors have any financial interests to disclose.

References

1. Brinkmann R, Roider J, Birngruber R (2006) Selective retina therapy (SRT): a review on methods, techniques, preclinical and first clinical results. Bull Soc Belge Ophtalmol (302):51–69
2. Brinkmann R, Huttmann G, Rogener J, Roider J, Birngruber R, Lin CP (2000) Origin of retinal pigment epithelium cell damage by pulsed laser irradiance in the nanosecond to microsecond time regimen. Lasers Surg Med 27(5):451–464
3. Kim HD, Han JW, Ohn YH, Brinkmann R, Park TK (2014) Functional evaluation using multifocal electroretinogram after selective retina therapy with a microsecond-pulsed laser. Invest Ophthalmol Vis Sci 56(1):122–131
4. Park YG, Seifert E, Roh YJ, Theisen-Kunde D, Kang S, Brinkmann R (2014) Tissue response of selective retina therapy by means of a feedback-controlled energy ramping mode. Clin Exp Ophthalmol 42(9):846–855
5. Framme C, Walter A, Prahs P et al (2009) Structural changes of the retina after conventional laser photocoagulation and selective retina treatment (SRT) in spectral domain OCT. Curr Eye Res 34(7):568–579
6. Framme C, Schuele G, Kobuch K, Flucke B, Birngruber R, Brinkmann R (2008) Investigation of selective retina treatment (SRT) by means of 8 ns laser pulses in a rabbit model. Lasers Surg Med 40(1):20–27
7. Elsner H, Porksen E, Klatt C et al (2006) Selective retina therapy in patients with central serous chorioretinopathy. Graefes Arch Clin Exp Ophthalmol 244(12):1638–1645
8. Klatt C, Saeger M, Oppermann T et al (2011) Selective retina therapy for acute central serous chorioretinopathy. Br J Ophthalmol 95(1):83–88
9. Koinzer S, Elsner H, Klatt C et al (2008) Selective retina therapy (SRT) of chronic subfoveal fluid after surgery of rhegmatogenous retinal detachment: three case reports. Graefes Arch Clin Exp Ophthalmol 246(10):1373–1378
10. Prahs P, Walter A, Regler R et al (2010) Selective retina therapy (SRT) in patients with geographic atrophy due to age-related macular degeneration. Graefes Arch Clin Exp Ophthalmol 248(5):651–658
11. Roider J, Liew SH, Klatt C et al (2010) Selective retina therapy (SRT) for clinically significant diabetic macular edema. Graefes Arch Clin Exp Ophthalmol 248(9):1263–1272

12. Colome J, Ruiz-Moreno JM, Montero JA, Fernandez E (2007) Diode laser-induced mitosis in the rabbit retinal pigment epithelium. Ophthalmic Surg Lasers Imaging 38(6):484–490
13. Framme C, Kobuch K, Eckert E, Monzer J, Roider J (2002) RPE in perfusion tissue culture and its response to laser application. Preliminary report. Ophthalmologica 216(5):320–328
14. Lee SH, Kim HD, Park YJ, Ohn YH, Park TK (2015) Time-dependent changes of cell proliferation after laser photocoagulation in mouse Chorioretinal tissue. Invest Ophthalmol Vis Sci 56(4): 2696–2708
15. Tababat-Khani P, Berglund LM, Agardh CD, Gomez MF, Agardh E (2013) Photocoagulation of human retinal pigment epithelial cells in vitro: evaluation of necrosis, apoptosis, cell migration, cell proliferation and expression of tissue repairing and cytoprotective genes. PLoS One 8(8):e70465
16. Chidlow G, Shibeeb O, Plunkett M, Casson RJ, Wood JP (2013) Glial cell and inflammatory responses to retinal laser treatment: comparison of a conventional photocoagulator and a novel, 3-nanosecond pulse laser. Invest Ophthalmol Vis Sci 54(3):2319–2332
17. Lehnardt S (2010) Innate immunity and neuroinflammation in the CNS: the role of microglia in toll-like receptor-mediated neuronal injury. Glia 58(3):253–263
18. Mainster MA, White TJ, Tips JH, Wilson PW (1970) Retinal-temperature increases produced by intense light sources. J Opt Soc Am 60(2):264–270
19. Wood JP, Shibeeb O, Plunkett M, Casson RJ, Chidlow G (2013) Retinal damage profiles and neuronal effects of laser treatment: comparison of a conventional photocoagulator and a novel 3-nanosecond pulse laser. Invest Ophthalmol Vis Sci 54(3):2305–2318
20. Neumanna J, Brinkmann R (2008) Self-limited growth of laser-induced vapor bubbles around single microabsorbers. Am Inst Phys 93
21. Kim HD, Jang SY, Lee SH et al (2016) Retinal pigment epithelium responses to selective retina therapy in mouse eyes. Invest Ophthalmol Vis Sci 57(7):3486–3495
22. Tackenberg MA, Tucker BA, Swift JS et al (2009) Muller cell activation, proliferation and migration following laser injury. Mol Vis 15:1886–1896
23. Krady JK, Basu A, Allen CM et al (2005) Minocycline reduces proinflammatory cytokine expression, microglial activation, and caspase-3 activation in a rodent model of diabetic retinopathy. Diabetes 54(5):1559–1565
24. BenEzra D, Hemo I, Maftzir G (1990) In vivo angiogenic activity of interleukins. Arch Ophthalmol 108(4):573–576
25. Shimura M, Yasuda K, Nakazawa T et al (2009) Panretinal photocoagulation induces pro-inflammatory cytokines and macular thickening in high-risk proliferative diabetic retinopathy. Graefes Arch Clin Exp Ophthalmol 247(12):1617–1624
26. Carmi Y, Voronov E, Dotan S et al (2009) The role of macrophage-derived IL-1 in induction and maintenance of angiogenesis. J Immunol 183(7):4705–4714
27. Lavalette S, Raoul W, Houssier M et al (2011) Interleukin-1beta inhibition prevents choroidal neovascularization and does not exacerbate photoreceptor degeneration. Am J Pathol 178(5): 2416–2423
28. Nelson CM, Ackerman KM, O'Hayer P, Bailey TJ, Gorsuch RA, Hyde DR (2013) Tumor necrosis factor-alpha is produced by dying retinal neurons and is required for Muller glia proliferation during zebrafish retinal regeneration. J Neurosci 33(15):6524–6539
29. Oliveira RG, Ferreira AP, Cortes AJ, Aarestrup BJ, Andrade LC, Aarestrup FM (2013) Low-level laser reduces the production of TNF-alpha, IFN-gamma, and IL-10 induced by OVA. Lasers Med Sci 28(6):1519–1525
30. Shi X, Semkova I, Muther PS, Dell S, Kociok N, Joussen AM (2006) Inhibition of TNF-alpha reduces laser-induced choroidal neovascularization. Exp Eye Res 83(6):1325–1334
31. Lee J, Choi JH, Joo CK (2013) TGF-beta1 regulates cell fate during epithelial-mesenchymal transition by upregulating survivin. Cell Death Dis 4:e714
32. Ie D, Gordon LW, Glaser BM, Pena RA (1994) Transforming growth factor-beta 2 levels increase following retinal laser photocoagulation. Curr Eye Res 13(10):743–746
33. Yamamoto C, Ogata N, Yi X et al (1998) Immunolocalization of transforming growth factor beta during wound repair in rat retina after laser photocoagulation. Graefes Arch Clin Exp Ophthalmol 236(1):41–46
34. Ishida K, Yoshimura N, Yoshida M, Honda Y (1998) Upregulation of transforming growth factor-beta after panretinal photocoagulation. Invest Ophthalmol Vis Sci 39(5):801–807
35. Ito A, Hirano Y, Nozaki M, Ashikari M, Sugitani K, Ogura Y (2015) Short pulse laser induces less inflammatory cytokines in the murine retina after laser photocoagulation. Ophthalmic Res 53(2):65–73
36. Ogata N, Ando A, Uyama M, Matsumura M (2001) Expression of cytokines and transcription factors in photocoagulated human retinal pigment epithelial cells. Graefes Arch Clin Exp Ophthalmol 239(2):87–95
37. Er H, Doganay S, Turkoz Y et al (2000) The levels of cytokines and nitric oxide in rabbit vitreous humor after retinal laser photocoagulation. Ophthalmic Surg Lasers 31(6):479–483
38. Jobling AI, Guymer RH, Vessey KA et al (2015) Nanosecond laser therapy reverses pathologic and molecular changes in age-related macular degeneration without retinal damage. FASEB J 29(2):696–710
39. Schuele G, Rumohr M, Huettmann G, Brinkmann R (2005) RPE damage thresholds and mechanisms for laser exposure in the microsecond-to-millisecond time regimen. Invest Ophthalmol Vis Sci 46(2):714–719
40. Kelly MW (1997) Intracellular cavitation as a mechanism of short-pulse laser injury to the retinal pigment epithelium. PhD thesis. Tufts University. 231